

Frequency stability control method considering limited EDCPS

eISSN 2051-3305

Received on 23rd August 2018

Accepted on 19th September 2018

E-First on 24th January 2019

doi: 10.1049/joe.2018.8543

www.ietdl.org

Yi Hu¹, Xiaoru Wang¹ ✉, Dalin Chen¹, Yulong Che¹¹School of Electrical Engineering, Southwest Jiaotong University, Chengdu 610031, People's Republic of China

✉ E-mail: huangganghui@163.com

Abstract: Aiming at the problem of frequency stability of the asynchronous AC/DC hybrid power grid, a prediction model of post-disturbance steady frequency is proposed, which considers the emergency DC power support (EDCPS) and the frequency response of AC grids on both sides of the high-voltage DC (HVDC) link. This post-disturbance steady frequency of both AC grids can be predicted quickly by utilising the wide area measurement system data, and the desired amount of EDCPS can be calculated directly by using the setting value of the steady frequency for the disturbed AC grid. Then this study considers the fact that the voltage level of the AC buses at both ends of the HVDC system will affect the operation modes of the HVDC system, resulting in the limited EDCPS. Therefore, a calculation method of the actual EDCPS command for steady frequency control is proposed. It can automatically identify the actual operation mode of the post-disturbance HVDC system and calculate the actual EDCPS command corresponding to the desired EDCPS value. Simulations of a typical two-area AC/DC hybrid power grid are carried out to validate the effectiveness of the proposed method.

1 Introduction

China has a vast geographical area, and its energy distribution and load demand are asymmetric. Southwest China has abundant hydropower resources, and Northwest China has plenty of new energy sources, while load demand is mainly concentrated in the central or eastern regions [1, 2]. These characteristics of energy and load distribution make it necessary for China to carry out the long-distance and large-capacity power transmission. The high-voltage DC (HVDC) transmission system has obvious advantages in these aspects, due to which the HVDC interconnection has been rapidly applied in China, such as 'power transmission from west to east' and 'nationwide interconnection' [3–5]. However, with the synchronous power grid decreasing, the inertia of the power grid to be weakened, and the problem of grid frequency stability caused by large disturbance will be more pronounced. Therefore, the frequency stability of the AC/DC hybrid power system attracts more and more people's attention [6].

The HVDC system has the advantages of fast power regulation and large power regulation capacity [7, 8]. When the AC grid is disturbed, the HVDC system can change the transmission power for rapid emergency DC power support (EDCPS) [9] and play a role in the controlling of frequency stability [10–12]. Therefore, how to make the reasonable use of EDCPS for frequency stability control is the key to improve the frequency stability of the AC/DC hybrid power system.

Chen *et al.* [13] and Wang *et al.* [14] have studied the frequency characteristics and the frequency control strategy of the sending-end grid when the HVDC transmission system is in the islanded operation mode. In reference [6, 15–17], various types of additional controllers are designed by introducing the feedback signal of frequency deviation, so as to change the active power control commands of the HVDC system and control the frequency fluctuation of the power grid. The aforementioned research is merely based on the unilateral grid frequency and its controller parameters for frequency control. It does not consider the network characteristics and structure of the power grid. More importantly, the design of controller parameters is related to the system conditions and difficult to transplant, so the practical applicability of these methods is poor.

Therefore, based on the real-time information provided by the wide-area measurement system (WAMS), a prediction model of post-disturbance steady frequency for the AC/DC hybrid power

grid is proposed in this paper. The model can take into account the influence of the generator governors, loads, HVDC systems, and grid network on the frequency, and predict the AC grid frequency on both sides of the HVDC system simultaneously and rapidly. Using the prediction model, the calculation method of EDCPS for steady frequency control is deduced according to the frequency setting value.

Previously, the desired EDCPS effect can be achieved by directly using the calculated EDCPS value as HVDC's active power raising command by using the traditional EDCPS method. However, this paper considers that the actual EDCPS effect is related to the HVDC's operation mode, which depends on the AC bus voltage level on both sides. In the case of large disturbance, the large-scale transfer of the power flow may worsen the voltage level of AC buses, resulting in an abnormal operation mode of the HVDC system. In this case, the actual EDCPS is limited, and the transmission power of the HVDC system cannot effectively raise to the desired EDCPS value, nor can it achieve effective frequency stability control [18, 19].

Therefore, this paper aims to find an effective method which can accurately control the post-disturbance steady frequency to the desired value, regardless of the HVDC's operation mode after disturbance. Based on the quasi-steady-state model of the HVDC system, this paper finds out the AC bus voltage boundaries and the functional relationship between the actual EDCPS command and the desired EDCPS effect in each operation mode of the HVDC system. Then, a frequency stability control method considering limited EDCPS is proposed in this paper. Based on the steady frequency prediction model and the desired EDCPS value, the method can automatically identify the operation mode of the HVDC system and calculate the actual EDCPS command for obtaining the desired EDCPS effect in the current operation mode.

2 Basic converter station equations of the HVDC transmission system

The HVDC transmission system mainly consists of converter stations and DC line; the schematic diagram is shown in Fig. 1.

For a multi-bridge HVDC converter station, the quasi-steady-state model is as follows [20]:

$$E_{acu} = n_u V_{acu} \quad (1)$$

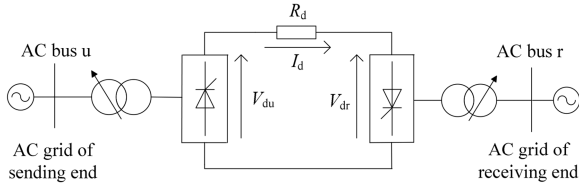


Fig. 1 Schematic of the HVDC transmission system

$$E_{acr} = n_r V_{acr} \quad (2)$$

$$V_{du} = N_u \left(\frac{3\sqrt{2}}{\pi} E_{acu} \cos \alpha - \frac{3}{\pi} X_{cu} I_d \right) \quad (3)$$

$$V_{dr} = N_r \left(\frac{3\sqrt{2}}{\pi} E_{acr} \cos \gamma - \frac{3}{\pi} X_{cr} I_d \right) \quad (4)$$

$$P_{du} = V_{du} I_d \quad (5)$$

$$P_{dr} = V_{dr} I_d \quad (6)$$

where E_{acu} and E_{acr} are the valve-side voltage of the rectifier and inverter station, respectively; V_{acu} and V_{acr} are the AC-side bus voltage of the rectifier and inverter station, respectively; n_u and n_r are the transformer ratios of the rectifier and inverter station, respectively; V_{du} and V_{dr} are the DC voltage of the rectifier-side and inverter-side of the DC line, respectively; N_u and N_r are the numbers of converter bridges in a series of the rectifier and inverter station, respectively; α and γ are the trigger delay angle and the extinction angle, respectively; X_{cu} and X_{cr} are the leakage reactance of transformer windings; I_d is the DC current; and P_{du} and P_{dr} are the injected active power of the rectifier and inverter station, respectively.

If the power loss of the DC line is considered, the rectifier-side DC voltage can be written as the inverter-side DC voltage plus the compensation voltage:

$$V_{du} = N_r \left(\frac{3\sqrt{2}}{\pi} E_{acr} \cos \gamma - \frac{3}{\pi} X_{cr} I_d \right) + R_d I_d \quad (7)$$

3 Node power increment equation of the power grid

3.1 Injected power equation of network nodes

The injected power equation of network nodes is as follows:

$$P_i = V_i \sum_{j=1}^n V_j (G_{ij} \cos \theta_{ij} + B_{ij} \sin \theta_{ij}) \quad (8)$$

$$Q_i = V_i \sum_{j=1}^n V_j (G_{ij} \sin \theta_{ij} - B_{ij} \cos \theta_{ij}) \quad (9)$$

where P_i and Q_i are the injected active and reactive power, respectively; V_i and V_j are the AC voltage amplitudes; G_{ij} and B_{ij} are the mutual admittances; θ_{ij} is the voltage phase angle difference; and n is the number of network nodes.

3.2 Electromagnetic power incremental equations of generator nodes

The power incremental equation of the i th generator is as follows:

$$\Delta P_{ei} = \Delta P_{mi} - \Delta P_{ai} \quad (10)$$

where ΔP_{ei} , ΔP_{mi} , and ΔP_{ai} are the electromagnetic, mechanical, and acceleration power incremental, respectively.

Considering the instantaneous moment and the steady-state after disturbance, (11) and (12) can be expressed as follows, due to $P_{ai} = 0$ at the steady state,

$$\Delta P_{mi} = P_{mi\infty} - P_{mi0^+} = -K_{Gi} \Delta \omega \quad (11)$$

$$\Delta P_{ai} = P_{ai\infty} - P_{ai0^+} = -P_{ai0^+} \quad (12)$$

where K_{Gi} is the frequency regulation coefficient of the i th generator, ω refers to the system inertia centre frequency except for special instructions in this paper, and the subscripts 0^+ and ∞ represent the instantaneous moment and the steady state after disturbance, respectively.

As the electromagnetic power output of the generator equals the injected power of the generator, (13) can be obtained from (10) to (12):

$$\Delta P_i = \Delta P_{ei} = -K_{Gi} \Delta \omega + P_{ai0^+} \quad (13)$$

Equation (13) can be expressed as

$$\Delta P_G = P_{i0^+} - P_{i\infty} - K_{Gi} \Delta \omega + P_{ai0^+} = 0 \quad (14)$$

3.3 Power increment equations of load nodes

The increment equation of the j th load node can be obtained as follows by considering that the consumed power is equal to the negative injected power for the j th load node:

$$P_{j0^+} - P_{j\infty} = -p_{Lj0^+} + p_{Lj\infty} \quad (15)$$

$$Q_{j0^+} - Q_{j\infty} = -q_{Lj0^+} + q_{Lj\infty} \quad (16)$$

In this paper, the static load model with voltage and frequency dependence is considered as follows:

$$p_L = p_0 (\alpha_p + \beta_p V + \gamma_p V^2) (1 + K_{pf} \Delta \omega) \quad (17)$$

$$q_L = q_0 (\alpha_q + \beta_q V + \gamma_q V^2) (1 + K_{qf} \Delta \omega) \quad (18)$$

where p_0 and q_0 are the active and reactive power at the rated voltage and frequency, respectively; α_p , β_p , γ_p , α_q , β_q , and γ_q are the proportion of the constant power, constant current, and constant impedance part of the active and reactive load, respectively, satisfied with $\alpha_p + \beta_p + \gamma_p = 1$ and $\alpha_q + \beta_q + \gamma_q = 1$; K_p and K_q are the frequency factor of the active and reactive power; $\Delta \omega^*$ is the deviation between the actual and standard frequency of the load.

Equations (15) and (16) can be expressed as

$$\Delta P_L = P_{j0^+} - P_{j\infty} + p_{Lj0^+} - p_{Lj\infty} = 0 \quad (19)$$

$$\Delta Q_L = Q_{j0^+} - Q_{j\infty} + q_{Lj0^+} - q_{Lj\infty} = 0 \quad (20)$$

3.4 Power increment equations of DC nodes

Assuming the desired EDCPS for the rectifier-side and inverter-side of the k th HVDC system are ΔP_{duk}^* and ΔP_{drk}^* , respectively, the injected power increment equations of the AC bus on the rectifier-side and inverter-side of the HVDC system are as follows:

$$\Delta P_{uk} = p_{Luk0^+} - p_{Luk\infty} - \Delta P_{duk}^* \quad (21)$$

$$\Delta P_{rk} = p_{Lrk0^+} - p_{Lrk\infty} + \Delta P_{drk}^* \quad (22)$$

Considering the power loss of the DC line, ΔP_{duk}^* and ΔP_{drk}^* should satisfy (23) as well:

$$(P_{duko} + \Delta P_{duk}^*) = (P_{drko} + \Delta P_{drk}^*) + \left(\frac{P_{drko} + \Delta P_{drk}^*}{V_{dko}} \right)^2 R_{dk} \quad (23)$$

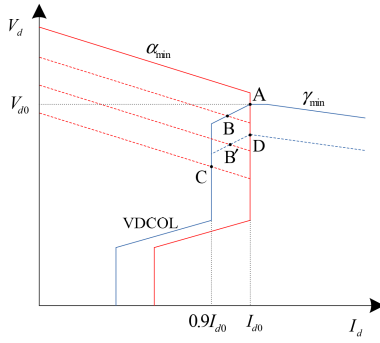


Fig. 2 Basic operating characteristics of the HVDC system

where P_{duko} and P_{drko} are the initial injected power of rectifier and inverter station, respectively; V_{dko} is the rated inverter-side DC voltage of the HVDC system.

Equations (21) and (22) can be expressed as follows:

$$\Delta P_U = P_{uko^+} - P_{uk\infty} + p_{Luko^+} - p_{Luk\infty} - \Delta P_{duk}^* = 0 \quad (24)$$

$$\Delta P_R = P_{rko^+} - P_{rk\infty} + p_{Lrko^+} - p_{Lrk\infty} + \Delta P_{drk}^* = 0 \quad (25)$$

4 Prediction model and control method of the steady frequency after disturbance

4.1 Steady frequency prediction model of the AC/DC hybrid power grid

When ΔP_{du}^* and ΔP_{dr}^* are given in (24) and (25), the frequency prediction model of the AC/DC hybrid power grid can be established by using the power increment equation of the system node presented in the previous section. By combining (14), (19), (20), (24), and (25), the correction equations of the frequency prediction model can be obtained as follows:

$$\begin{bmatrix} \Delta P_G \\ \Delta P_L \\ \Delta P_U \\ \Delta P_R \\ \Delta Q_L \end{bmatrix} = \begin{bmatrix} H_{GG} & H_{GL} & N_{GL} & A_{11} & A_{12} \\ H_{LG} & H_{LL} & N_{LL} & A_{21} & A_{22} \\ H_{UG} & H_{GG} & N_{UL} & A_{31} & A_{32} \\ H_{RG} & H_{GG} & N_{RL} & A_{41} & A_{42} \\ J_{LG} & J_{LL} & L_{LL} & A_{51} & A_{52} \end{bmatrix} \begin{bmatrix} \Delta \theta_G \\ \Delta \theta_L \\ \Delta V_L \\ \Delta \omega_1 \\ \Delta \omega_2 \end{bmatrix} \quad (26)$$

where ΔP_G , ΔP_L , ΔP_U , and ΔP_R represent the active power increment of the generator, load, rectifier-side and inverter-side DC nodes, respectively; ΔQ_L represents the reactive power incremental of load nodes; $\Delta \theta_G$, $\Delta \theta_L$, ΔV_L , $\Delta \omega_1$, and $\Delta \omega_2$ are the variations of the voltage phase angle, voltage amplitude, and inertia centre frequencies of the rectifier-side and inverter-side AC grid, respectively. The expressions of H , N , J , L and the Jacobi matrix elements are the same with the power flow calculation. The matrix A_{11} , A_{12} , A_{21} , A_{22} , A_{31} , A_{32} , A_{41} , A_{42} , A_{51} , A_{52} are the derivative of ΔP_G , ΔP_L , ΔP_U , ΔP_R , ΔQ_L to $\Delta \omega_1$, $\Delta \omega_2$ respectively, and the details of the power increment and Jacobian matrix elements are shown in Appendix A.

The aforementioned prediction model can be iteratively solved by the Newton-Raphson method, and finally the steady frequency of the AC/DC hybrid power grid can be predicted after considering the EDCPS.

4.2 Frequency stability control method considering the limited EDCPS for the AC/DC hybrid power grid after disturbance

When the steady frequency setting value ω_{set} of the disturbed AC grid (the receiving end grid) is given, a new correction (27) can be further derived by modifying the correction equation of the frequency prediction model.

$$\begin{bmatrix} \Delta P_G \\ \Delta P_L \\ \Delta P_U \\ \Delta P_R \\ \Delta Q_L \end{bmatrix} = \begin{bmatrix} H_{GG} & H_{GL} & N_{GL} & B_{11} & 0 \\ H_{LG} & H_{LL} & N_{LL} & B_{21} & 0 \\ H_{UG} & H_{GG} & N_{UL} & B_{31} & B_{32} \\ H_{RG} & H_{GG} & N_{RL} & B_{41} & B_{42} \\ J_{LG} & J_{LL} & L_{LL} & B_{51} & 0 \end{bmatrix} \begin{bmatrix} \Delta \theta_G \\ \Delta \theta_L \\ \Delta V_L \\ \Delta \omega_1 \\ \Delta P_{du}^* \end{bmatrix} \quad (27)$$

where B_{11} , B_{21} , B_{31} , B_{32} , B_{41} , B_{42} , and B_{51} are the derivatives of ΔP_G , ΔP_L , ΔP_U , ΔP_R , ΔQ_L to $\Delta \omega_1$, ΔP_{du}^* , respectively, and the details of power increment and Jacobian matrix elements are shown in Appendix B.

Therefore, by solving (27) iteratively, the desired EDCPS (ΔP_{du}^*), the steady frequency of the sending-end grid ($\Delta \omega_1$), and all node voltages after the disturbance can be obtained.

This paper considers that the effect of EDCPS is related to the operation mode of the HVDC system, and ultimately depends on the AC bus voltage level on both sides. Therefore, it is necessary to distinguish the operation mode according to the AC bus voltage and calculate the actual EDCPS command according to the desired EDCPS effect in the current operation mode.

In order to accurately analyse the influence of the AC bus voltage on the EDCPS, this paper considers the most common control mode of the HVDC system as constant current control of the rectifier and constant voltage control of the inverter [21]. Without considering the impact of the voltage-dependent current order limiter, there are four possible operation modes of the HVDC system based on the AC bus voltage levels, which are shown in Fig. 2.

Mode A: In this mode, the rectifier and inverter station of the HVDC system adopt the constant current control and constant voltage control modes, respectively, and run at the point A in Fig. 2.

Assuming that the actual command of EDCPS is ΔP_{duref}^* , the desired transmission of active power and its control command of the rectifier station are as follows:

$$\begin{cases} P_{du}^* = P_{duo} + \Delta P_{du}^* \\ P_{duref} = P_{duo} + \Delta P_{duref}^* \end{cases} \quad (28)$$

According to the operating characteristic of mode A, the functional relationship between the active power control command and the desired active power transmission can be obtained:

$$P_{durefA} = (V_{d0} + R_d I_{d0A}) I_{d0A} = V_{duA} I_{dA} = P_{du}^* \quad (29)$$

where the subscript A indicates the electrical variables in the operation mode A, and the subscripts B, C and D are synonymous with A in the following text.

According to the basic characteristics of the operation mode A and the quasi-steady-state model of the HVDC system, the AC bus voltage boundary conditions of the current operation mode are obtained:

$$\begin{cases} V_{d0A} = N_r \left(\frac{3\sqrt{2}}{\pi} E_{acr} \cos \gamma_A - \frac{3}{\pi} X_{cr} I_{d0A} \right) \\ \gamma_A > \gamma_{min} \\ V_{d0} + R_d I_{d0A} = N_u \left(\frac{3\sqrt{2}}{\pi} E_{acu} \cos \alpha_A - \frac{3}{\pi} X_{cu} I_{d0A} \right) \\ \alpha_A > \alpha_{min} \end{cases} \quad (30)$$

where γ_{min} and α_{min} are the minimum trigger delay angle of the rectifier station and the minimum extinction angle of the inverter station, respectively.

Mode B: In this mode, the rectifier and inverter station of the HVDC system adopt the constant minimum trigger angle control and current deviation control modes, respectively, and run at the point B or B' in Fig. 2.

According to the operating characteristics of mode B, the functional relationship can be obtained:

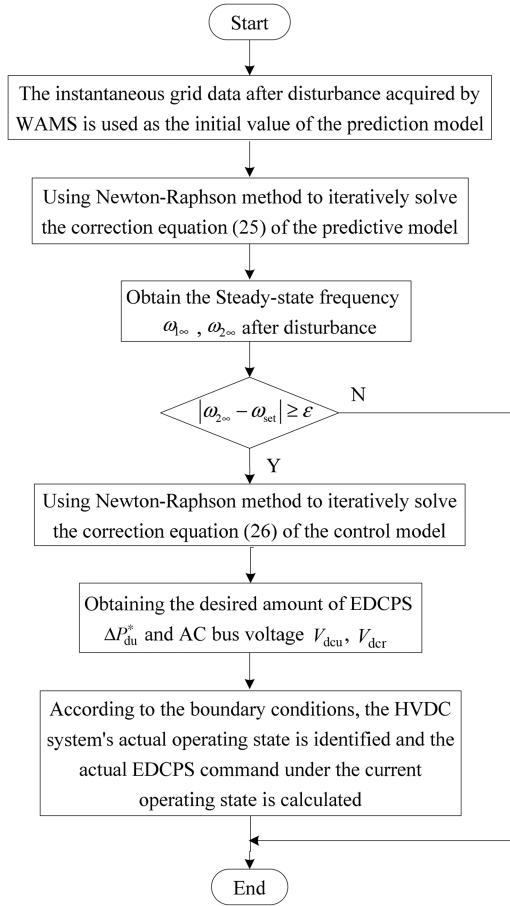


Fig. 3 Flowchart of the frequency stability control method considering the limited EDCPS

$$\begin{cases} V_{duB} = N_u \left(\frac{3\sqrt{2}}{\pi} E_{acu} \cos \alpha_{\min} - \frac{3}{\pi} X_{cu} I_{dB} \right) \\ P_{du}^* = V_{duB} I_{dB} \\ N_r \left(\frac{3\sqrt{2}}{\pi} E_{acr} \cos \gamma_B - \frac{3}{\pi} X_{cr} I_{dB} \right) + R_d I_{dB} = V_{duB} \\ V_{d0} = N_r \left(\frac{3\sqrt{2}}{\pi} E_{acr} \cos \gamma_{ref1B} - \frac{3}{\pi} X_{cr} I_{d0B} \right) \\ \gamma_{ref2} = \gamma_{\min} \\ \gamma_B = \max \{ \gamma_{ref1B}, \gamma_{ref2} \} + K_c \frac{I_{d0B} - I_{dB}}{I_{d0B}} \\ P_{durefB} = (V_{d0} + R_d I_{d0B}) I_{d0B} \end{cases} \quad (31)$$

In this mode, the AC bus voltage boundary conditions are as follows:

$$\begin{cases} V_{duB} = N_u \left(\frac{3\sqrt{2}}{\pi} E_{acu} \cos \alpha_{\min} - \frac{3}{\pi} X_{cu} I_{dB} \right) \\ N_r \left(\frac{3\sqrt{2}}{\pi} E_{acr} \cos \gamma_B - \frac{3}{\pi} X_{cr} I_{dB} \right) + R_d I_{dB} = V_{duB} \\ \gamma_B = \max \{ \gamma_{ref1B}, \gamma_{ref2} \} + K_c \frac{I_{d0B} - I_{dB}}{I_{d0B}} \\ 0.9 I_{d0B} < I_{dB} < I_{d0B} \\ V_{drB} = N_u \left(\frac{3\sqrt{2}}{\pi} E_{acu} \cos \alpha_{\min} - \frac{3}{\pi} X_{cu} I_{dB} \right) - R_d I_{d0B} \\ V_{drB} < V_{d0} \end{cases} \quad (32)$$

Mode C: In this mode, the rectifier and inverter station of the HVDC system adopt the constant minimum trigger angle control and constant current control modes, respectively, and run at the point C in Fig. 2.

According to the operating characteristics of mode C, the functional relationship can be obtained:

$$\begin{cases} V_{duC} = N_u \left(\frac{3\sqrt{2}}{\pi} E_{acu} \cos \alpha_{\min} - \frac{3}{\pi} X_{cu} 0.9 I_{d0C} \right) \\ P_{du}^* = V_{duC} 0.9 I_{d0C} \\ P_{durefC} = (V_{d0} + R_d I_{d0C}) I_{d0C} \end{cases} \quad (33)$$

In this mode, the AC bus voltage boundary conditions are as follows:

$$\begin{cases} V_{d0} = N_r \left(\frac{3\sqrt{2}}{\pi} E_{acr} \cos \gamma_{ref1C} - \frac{3}{\pi} X_{cr} I_{d0C} \right) \\ \gamma_{ref2} = \gamma_{\min} \\ \gamma'_C = \max \{ \gamma_{ref1C}, \gamma_{ref2} \} + K_c \frac{I_{d0C} - 0.9 I_{d0C}}{I_{d0C}} \\ V'_{drC} = N_r \left(\frac{3\sqrt{2}}{\pi} E_{acr} \cos \gamma'_C - \frac{3}{\pi} X_{cr} (0.9 I_{d0C}) \right) \\ N_u \left(\frac{3\sqrt{2}}{\pi} E_{acu} \cos \alpha_{\min} - \frac{3}{\pi} X_{cu} (0.9 I_{d0C}) \right) - R_d (0.9 I_{d0C}) < V'_{drC} \end{cases} \quad (34)$$

Mode D: In this mode, the rectifier and inverter station of the HVDC system adopt the constant current control and minimum extinction angle control modes, respectively, and run at the point D in Fig. 2.

According to the operating characteristics of mode D, the functional relationship can be obtained:

$$\begin{cases} V_{duD} = N_r \left(\frac{3\sqrt{2}}{\pi} E_{acr} \cos \gamma_{\min} - \frac{3}{\pi} X_{cr} I_{d0D} \right) + R_d I_{d0D} \\ P_{du}^* = V_{duD} I_{d0D} \\ P_{durefD} = (V_{d0} + R_d I_{d0D}) I_{d0D} \end{cases} \quad (35)$$

In this mode, the AC bus voltage boundary conditions are as follows:

$$\begin{cases} V_{drD} = N_r \left(\frac{3\sqrt{2}}{\pi} E_{acr} \cos \gamma_{\min} - \frac{3}{\pi} X_{cr} I_{d0D} \right) \\ V_{drD} + R_d I_{d0D} = N_u \left(\frac{3\sqrt{2}}{\pi} E_{acu} \cos \alpha_D - \frac{3}{\pi} X_{cu} I_{d0D} \right) \\ \alpha_D > \alpha_{\min} \\ N_r \left(\frac{3\sqrt{2}}{\pi} E_{acr} \cos \gamma_{\min} - \frac{3}{\pi} X_{cr} I_{d0D} \right) < V_{d0D} \end{cases} \quad (36)$$

According to these function relationships and their corresponding boundary conditions, the flowchart of the frequency stability control for the AC/DC hybrid power system with limited EDCPS is shown in Fig. 3.

5 Simulation analysis

In this paper, the proposed frequency stability control method for the AC/DC hybrid power grid is realised by MATLAB, and the simulation system is built in Power System Simulator for Engineering (PSS/E). The instantaneous moment data of the simulation system in PSS/E is used as the WAMS data after the disturbance. Finally, the PSS/E simulation results are used to verify the control effect of the proposed method.

5.1 Simulation system

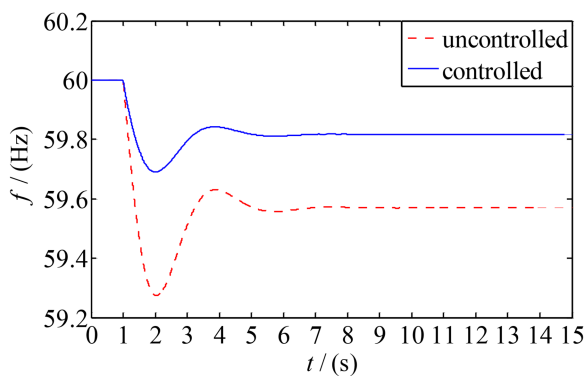
In this paper, a typical asynchronous AC/DC hybrid power grid is built in PSS/E. As shown in Fig. C1, the hybrid power grid consists of the AC grid A, AC grid B, and two HVDC systems. Grids A and B are, respectively, the sending-end and receiving-end AC grid, and both of them are modified from the IEEE39 system.

Table 1 Basic parameters of the HVDC transmission system

Parameter name	Parameter value, pu	Parameter name	Parameter value, pu
N_u	2	N_r	2
n_u	10.391	n_r	10.479
X_{cu}	0.013	X_{cr}	0.013
R_d	0.01	P_{dr0}	8
α_{min}	5	γ_{min}	15
I_{d0}	1.6	U_{d0}	5

Table 2 Comparison of the post-disturbance steady frequency of the two grids

Grid name	Prediction, Hz	PSS/E simulation, Hz	Absolute error, Hz	Relative error, %
grid A	60.0186	59.9995	0.0310	0.0517
grid B	59.5471	59.5696	0.0225	0.0378

**Fig. 4** Comparison of the frequency curve of the grid B with and without the proposed control

The two HVDC lines are, respectively, connected with Node 3A and Node 3B, Node 24A and Node 24B. Both of them adopt the control mode: rectifier with constant current control and inverter with constant voltage control. In this paper, the reference power of the HVDC system is selected as 100 MW, and the reference voltage is selected as 500 kV. The basic parameters of the HVDC system are shown in Table 1.

5.2 Case study

In order to verify the correctness and effectiveness of the proposed method, the case studies are given in different operation modes of the HVDC system.

Case 1: The HVDC system in the normal operation mode

Condition: When the AC/DC hybrid power system is in stable operation at the time of $t = 1$ s, the active power of the load node B18 suddenly increases by 300 MW.

According to the condition of this case, the steady frequency after disturbance obtained by PSS/E simulation and the result calculated by the prediction model are compared in Table 2.

According to Table 2, it can be seen that the steady frequency of the AC/DC hybrid power system calculated by the prediction model is basically consistent with the PSS/E simulation result, and the absolute error and relative error are very small. This shows that the prediction model proposed in this paper has a high accuracy and lays a good foundation for the steady frequency control.

Assuming that the setting value of the post-disturbance steady frequency of grid B is $\omega_{set} = 59.8$ Hz, it can be seen from Table 2 that the predicted steady frequency is obviously lower than the setting value. Therefore, the proposed method is used to calculate the result of the control in this case, as shown in Table 3:

It can be seen from Table 3 that the operation mode of the HVDC system is the constant current control of the rectifier station

Table 3 Calculation results of the proposed method in this case condition

Calculation results		Value
AC bus voltage, pu	rectifier side	0.9760
	inverter side	1.0269
steady frequency, Hz	grid A	59.7454
	grid B	59.8000
operation mode of HVDC		A
desired EDCPS, pu		1.7742
actual EDCPS command value, pu		1.7742

Table 4 Comparison of the post-disturbance steady frequency after the EDCPS implementation

Grid name	Proposed method, Hz	PSS/E simulation, Hz	Absolute error, Hz	Relative error, %
grid A	59.7454	59.7334	0.0120	0.0201
grid B	59.8000	59.8169	0.0169	0.0283

Table 5 Calculation results of the proposed method in this case condition

Calculation results		Value
AC bus voltage, pu	rectifier side	0.9430
	inverter side	1.0298
steady frequency, Hz	grid A	59.7321
	grid B	59.8000
operation mode of HVDC		B
desired EDCPS, pu		1.7762
actual EDCPS command value, pu		2.6940

and the constant voltage control of the inverter station under this case condition. So in this case, the actual EDCPS command calculated by the proposed method is the same as the desired EDCPS. In order to validate the correctness of the calculation results, the actual EDCPS command is used as the active power control command of the HVDC system in the PSS/E simulation. The control results are shown in Table 4 and Fig. 4.

As can be seen from Table 4 and Fig. 4, after the actual EDCPS command value or the desired EDCPS value is used as the active power control command of the HVDC system in PSS/E simulation, the post-disturbance steady frequency of grid B can be improved and accurately restored to the setting value. The error of the control result is small, which verifies that the proposed method has a good control effect under the normal operation mode of the HVDC system.

Case 2: The HVDC system is in the abnormal operation mode

Condition 1: When the AC/DC hybrid power system is in stable operation at the time of $t = 1$ s, the active power of the load node B18 suddenly increases by 300 MW, and the reactive power of the load node A18 suddenly increases by 300 MVar.

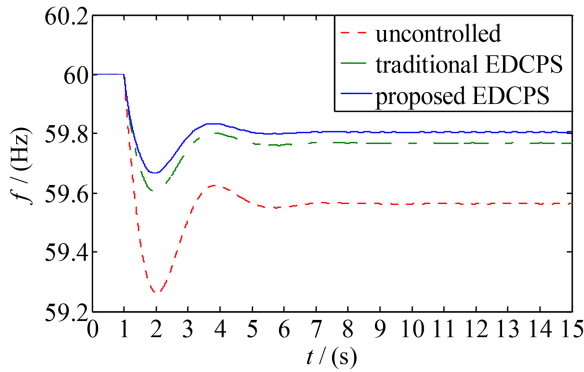
According to $\omega_{set} = 59.8$ Hz, the results are calculated by the proposed method and shown in Table 5.

It can be seen from Table 5 that the operation mode of the HVDC system is the constant minimum trigger angle control of the rectifier station and the current deviation control of the inverter station under this case condition. So the actual EDCPS command is 91.78 MW more than the desired EDCPS value. Using the actual EDCPS command and the desired EDCPS value as the HVDC active power raising command, respectively, the control effect comparison of PSS/E simulations are shown in Table 6 and Fig. 5 below.

As can be seen from Table 7 and Fig. 6, when the traditional EDCPS method is implemented, the post-disturbance steady frequency of grid B cannot recover to the setting value. However, the proposed EDCPS method can restore the post-disturbance steady frequency to the setting value with a small error. This case verifies that the proposed method can still improve the post-

Table 6 Comparison of post-disturbance steady frequency after EDCPS implementation

Comparative items	Proposed EDCPS		Traditional EDCPS	
	Grid A	Grid B	Grid A	Grid B
steady frequency, Hz	59.7254	59.8051	59.7876	59.7677
absolute error, Hz	0.0218	0.0051	0.0404	0.0323
relative error, %	0.0365	0.0085	0.0676	0.0540

**Fig. 5** Comparison of the frequency curve of the grid B with the different EDCPS

disturbance steady frequency stability when the HVDC system is in the abnormal operation mode.

Condition 2: When the AC/DC hybrid power system is in stable operation at the time of $t = 1$ s, the active power of the load node B18 suddenly increases by 300 MW and reactive power by 300 MVar; the reactive power of the load node A18 suddenly decreases by 300 MVar.

According to $\omega_{set} = 59.8$ Hz, the calculation results of the proposed method are shown in Table 8.

It can be seen from Table 8 that the control mode of the HVDC system is the constant current control of the rectifier station and the minimum extinction angle control of the inverter station, and the actual EDCPS command is 28.26 MW more than the desired EDCPS value. Using the actual EDCPS command and the desired EDCPS value as the active power raising command, respectively, the comparison of the control effect is shown in Table 6 and Fig. 5.

As can be seen from Table 6 and Fig. 5, the proposed EDCPS method can restore the post-disturbance steady frequency to the setting value more accurately than the traditional EDCPS method. Therefore, it is verified once again that the proposed EDCPS calculation method has good effectiveness and applicability when the HVDC system is in an abnormal operation mode after many large disturbances.

6 Conclusions

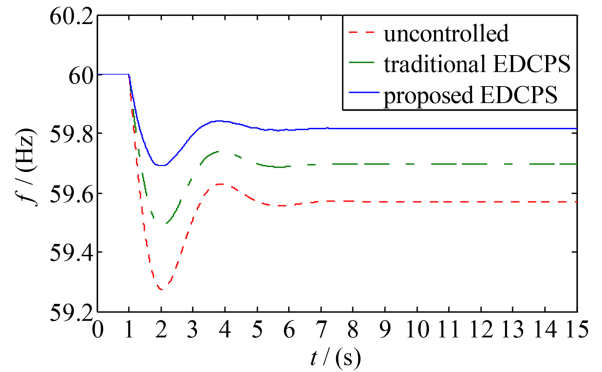
A prediction model of the post-disturbance steady frequency for the AC/DC hybrid power system is proposed in this paper, which takes into consideration the EDCPS and the frequency response of the AC grids on both sides of the HVDC system. Based on the model, the calculation method of EDCPS for the steady frequency control is deduced. This paper considers that the desired EDCPS will be limited in the abnormal operation modes of the HVDC system. Therefore, a calculation method of the actual EDCPS command for steady frequency control is proposed. In the case studies, the applicability, effectiveness, and superiority of the proposed method are verified by comparing the results of PSS/E simulations.

7 Acknowledgments

This work was supported by China Postdoctoral Science Foundation funded projects (Operational Characteristics Analysis and Stability Control for the Southwest Power Grid with Multi-HVDC Links).

Table 7 Comparison of post-disturbance steady frequency after EDCPS implementation

Comparative items	Proposed EDCPS		Traditional EDCPS	
	Grid A	Grid B	Grid A	Grid B
steady frequency, Hz	59.7057	59.8173	59.8660	59.6966
absolute error, Hz	0.0264	0.0173	0.1339	0.1034
relative error, %	0.0442	0.0289	0.2242	0.1729

**Fig. 6** Comparison of the frequency curve of the grid B with different EDCPS**Table 8** Calculation results of the proposed method in this case condition

Calculation results			Value
AC bus voltage, pu	rectifier side		0.9933
	inverter side		0.9748
steady frequency, Hz	grid A		59.7472
	grid B		59.8000
operation mode of HVDC			D
desired EDCPS, pu			1.7745
actual EDCPS command value, pu			2.0571

8 References

- [1] Zhang, N., Zhou, Q., Tang, J., *et al.*: 'Unit commitment model and algorithm for receiving-end power grid in hybrid AC/DC system', *Autom. Electr. Power Syst.*, 2017, **41**, (11), pp. 77–84
- [2] Zeng, M., Li, H., Ma, M., *et al.*: 'Review on transaction status and relevant policies of southern route in China's west-east power transmission', *Renew. Energy*, 2013, **60**, (60), pp. 454–461
- [3] Li, Q., Liu, M., Liu, H.: 'Piecewise normalized normal constraint method applied to minimization of voltage deviation and active power loss in an AC-DC hybrid power system', *IEEE Trans. Power Syst.*, 2015, **30**, (3), pp. 1243–1251
- [4] Qu, W., Jiang, J., Zhao, Q., *et al.*: 'Subsynchronous oscillation and its practical mitigation project at the Hulun Buir power plant generating for a Chinese extra-high-voltage AC and DC hybrid transmission network', *IET Gener. Transm. Distrib.*, 2016, **10**, (4), pp. 949–954
- [5] Chen, X., Liu, B., Ren, D., *et al.*: 'Study on influence of DC power transfer on AC voltages in hybrid AC/DC system', *Power Syst. Technol.*, 2016, **40**, (7), pp. 1957–1961
- [6] Zhu, H., Luo, L.: 'Improving frequency stability of parallel AC-DC hybrid systems by power modulation strategy of HVDC link', *Proc. CSEE*, 2012, **32**, (16), pp. 36–43
- [7] Liu, C., Zhao, Y., Li, G., *et al.*: 'Design of LCC HVDC wide-area emergency power support control based on adaptive dynamic surface control', *IET Gener. Transm. Distrib.*, 2017, **11**, (13), pp. 3236–3245
- [8] Zhou, J., Liu, C., Zhao, J.: 'Transient and dynamic stability enhancement by coordination control of HVDC links of northwest ac/dc grid'. Proc. 2016 China Int. Conf. on Electricity Distribution, Xi'an, China, Aug. 2016, pp. 1–5
- [9] Liu, X., Xie, H., Wang, H., *et al.*: 'Emergency DC power support in parallel AC/DC power system'. Proc. 2013 Int. Conf. on Mechatronics and Automatic Control Systems, Hangzhou, China, Aug. 2013, pp. 525–532
- [10] Li, H., Yuan, Y., Zhang, X., *et al.*: 'Analysis of frequency emergency control characteristics of UHV AC/DC large receiving end power grid', *J. Eng.*, 2017, **1**, (1), pp. 1–5
- [11] Lin, Q., Li, X., Hu, N., *et al.*: 'A multi-agent based emergency DC power support strategy', *Power Syst. Technol.*, 2014, **38**, (5), pp. 1150–1155
- [12] Wen, Y., Chung, C. Y., Ye, X.: 'Enhancing frequency stability of asynchronous grids interconnected with HVDC links', *IEEE Trans. Power Syst.*, 2017, **PP**, (99), pp. 1–1
- [13] Chen, Y., Cheng, Z., Zhang, K., *et al.*: 'Frequency regulation strategy for islanding operation of HVDC', *Proc. CSEE*, 2013, **33**, (4), pp. 96–102

- [14] Wang, H., Han, M., Fan, Y., *et al.*: 'Sending end frequency characteristics under islanded operation mode of HVDC transmission system from Hulun Buir to Liaoning and corresponding control strategy', *Power Syst. Technol.*, 2013, **37**, (5), pp. 1401–1406
- [15] Ngamroo, I.: 'A stabilization of frequency oscillations using a power modulation control of HVDC link in a parallel AC-DC interconnected system', *Proc. the Power Conversion Conf.-Osaka 2002*, Osaka, Japan, Aug. 2002, pp. 1405–1410
- [16] Andreasson, M., Wiget, R., Dimarogonas, D. V., *et al.*: 'Distributed primary frequency control through multi-terminal HVDC transmission systems', *Proc. 2015 American Control Conf.*, Chicago, IL, USA, July 2015, pp. 5029–5034
- [17] Tang, Y., Song, M., Wang, Q., *et al.*: 'Frequency control strategy for wind-thermal-bundled power system with HVDC line', *Proc. 2015 IEEE Int. Conf. on Cyber Technology in Automation, Control, and Intelligent Systems*, Shenyang, China, June 2015, pp. 767–772
- [18] Wang, K., Yang, S., Yao, J., *et al.*: 'Emergency DC power support with reactive power coordinated control for multi-circuit HVDC systems', *Autom. Electr. Power Syst.*, 2011, **35**, (18), pp. 103–107
- [19] Weng, H., Xu, Z., Xu, F., *et al.*: 'Research on constraint factor of emergency power support of HVDC systems', *Proc. CSEE*, 2014, **34**, (10), pp. 1519–1527
- [20] Xu, Z.: 'Dynamic behavior analysis of AC/DC power systems' (China Machine Press, Beijing, China, 2004, 1st edn.), pp. 31–35
- [21] Zhao, W.: 'High voltage direct current transmission engineering technology' (China Electric Power Press, Beijing China, 2004, 2nd edn.), pp. 97–103

9 Appendix A

The specific expressions of ΔP_G , ΔP_L , ΔP_U , ΔP_R , and ΔQ_L in (26) are as follows:

$$\Delta P_{Gi} = P_{ei0^+} - V_{i\infty} \sum_{j=1}^n V_{j\infty} (G_{ij} \cos \theta_{ij\infty} + B_{ij} \sin \theta_{ij\infty}) - K_{Gi} (\omega_{\infty} - \omega_0^+) + P_{ai0^+} \quad (37)$$

$$\begin{aligned} \Delta P_{Li} &= p_{Li0^+} - V_{i\infty} \sum_{j=1}^n V_{j\infty} (G_{ij} \cos \theta_{ij\infty} + B_{ij} \sin \theta_{ij\infty}) \\ &\quad + p_0 (\alpha_p + \beta_p V_{0^+} + \gamma_p V_{0^+}^2) (1 + K_{pf} \omega_0^+) \\ &\quad - p_0 (\alpha_p + \beta_p V_{\infty} + \gamma_p V_{\infty}^2) (1 + K_{pf} \omega_{\infty}) \end{aligned} \quad (38)$$

$$\begin{aligned} \Delta P_{ui} &= p_{Lui0^+} - V_{i\infty} \sum_{j=1}^n V_{j\infty} (G_{ij} \cos \theta_{ij\infty} + B_{ij} \sin \theta_{ki\infty}) \\ &\quad + p_0 (\alpha_p + \beta_p V_{0^+} + \gamma_p V_{0^+}^2) (1 + K_{pf} \omega_0^+) \\ &\quad - p_0 (\alpha_p + \beta_p V_{\infty} + \gamma_p V_{\infty}^2) (1 + K_{pf} \omega_{\infty}) - \Delta P_{du}^* \end{aligned} \quad (39)$$

$$\begin{aligned} \Delta P_{ri} &= p_{Lri0^+} - V_{i\infty} \sum_{j=1}^n V_{j\infty} (G_{ij} \cos \theta_{ij\infty} + B_{ij} \sin \theta_{ij\infty}) \\ &\quad + p_0 (\alpha_p + \beta_p V_{0^+} + \gamma_p V_{0^+}^2) (1 + K_{pf} \omega_0^+) \\ &\quad - p_0 (\alpha_p + \beta_p V_{\infty} + \gamma_p V_{\infty}^2) (1 + K_{pf} \omega_{\infty}) \\ &\quad + \frac{\sqrt{(2R_d + V_{d0}^2)^2 + 4R_d V_{d0}^2 \Delta P_{du}^*} - (2R_d + V_{d0}^2)}{2R_d} \end{aligned} \quad (40)$$

$$\begin{aligned} \Delta Q_{Li} &= q_{Li0^+} - V_{i\infty} \sum_{j=1}^n V_{j\infty} (G_{ij} \sin \theta_{ij\infty} - B_{ij} \sin \theta_{ij\infty}) \\ &\quad + q_0 (\alpha_q + \beta_q V_{0^+} + \gamma_q V_{0^+}^2) (1 + K_{qf} \omega_0^+) \\ &\quad - q_0 (\alpha_q + \beta_q V_{\infty} + \gamma_q V_{\infty}^2) (1 + K_{qf} \omega_{\infty}) \end{aligned} \quad (41)$$

The elements of \mathbf{H} , \mathbf{N} , \mathbf{J} , and \mathbf{L} have the same meaning and form as the elements in the traditional power flow calculation, and are not described herein again. The elements of \mathbf{A} for the rectifier-side AC grid are as follows:

$$A_{11} = \frac{\partial \Delta P_{Gi}}{\partial \omega_1} = -K_{Gi} \quad (42)$$

$$A_{12} = \frac{\partial \Delta P_{Gi}}{\partial \omega_2} = 0$$

$$A_{21} = \frac{\partial \Delta P_{Li}}{\partial \omega_1} = -p_0 K_{pf} (\alpha_p + \beta_p V_{i\infty} + \gamma_p V_{i\infty}^2) \quad (43)$$

$$A_{22} = \frac{\partial \Delta P_{Li}}{\partial \omega_2} = 0$$

$$A_{31} = \frac{\partial \Delta Q_{Li}}{\partial \omega_1} = -q_0 K_{qf} (\alpha_q + \beta_q V_{i\infty} + \gamma_q V_{i\infty}^2) \quad (44)$$

$$A_{32} = \frac{\partial \Delta Q_{Li}}{\partial \omega_2} = 0$$

$$A_{31} = \frac{\partial \Delta P_{Ui}}{\partial \omega_1} = -p_0 K_{pf} (\alpha_p + \beta_p V_{i\infty} + \gamma_p V_{i\infty}^2) \quad (45)$$

$$A_{32} = \frac{\partial \Delta P_{Ui}}{\partial \omega_2} = 0$$

The elements of \mathbf{A} for the inverter-side AC grid are as follows:

$$A_{11} = \frac{\partial \Delta P_{Gi}}{\partial \omega_1} = 0 \quad (46)$$

$$A_{12} = \frac{\partial \Delta P_{Gi}}{\partial \omega_2} = -K_{Gi}$$

$$A_{21} = \frac{\partial \Delta P_{Li}}{\partial \omega_1} = 0 \quad (47)$$

$$A_{22} = \frac{\partial \Delta P_{Li}}{\partial \omega_2} = -p_0 K_{pf} (\alpha_p + \beta_p V_{i\infty} + \gamma_p V_{i\infty}^2)$$

$$A_{31} = \frac{\partial \Delta Q_{Li}}{\partial \omega_1} = 0 \quad (48)$$

$$A_{32} = \frac{\partial \Delta Q_{Li}}{\partial \omega_2} = -q_0 K_{qf} (\alpha_q + \beta_q V_{i\infty} + \gamma_q V_{i\infty}^2)$$

$$A_{41} = \frac{\partial \Delta P_{Ri}}{\partial \omega_1} = 0 \quad (49)$$

$$A_{42} = \frac{\partial \Delta P_{Ri}}{\partial \omega_2} = -p_0 K_{pf} (\alpha_p + \beta_p V_{i\infty} + \gamma_p V_{i\infty}^2)$$

10 Appendix B

The elements of \mathbf{H} , \mathbf{N} , \mathbf{J} , and \mathbf{L} have the same meaning and form as the elements in the traditional power flow calculation, and are not described herein again. The elements of \mathbf{B} are as follows:

$$B_{11} = \frac{\partial \Delta P_{Gi}}{\partial \omega_1} = -K_{Gi} \quad (50)$$

$$B_{21} = \frac{\partial \Delta P_{Li}}{\partial \omega_1} = -K_{pf} p_0 (\alpha_p + \beta_p V_{i\infty} + \gamma_p V_{i\infty}^2) \quad (51)$$

$$B_{31} = \frac{\partial \Delta P_{Ui}}{\partial \omega_1} = -p_0 K_{pf} (\alpha_p + \beta_p V_{i\infty} + \gamma_p V_{i\infty}^2) \quad (52)$$

$$B_{32} = \frac{\partial \Delta P_{Ui}}{\partial \Delta P_{du}^*} = -1 \quad (53)$$

$$B_{41} = \frac{\partial \Delta P_{Ri}}{\partial \omega_1} = -p_0 K_{pf} (\alpha_p + \beta_p V_{i\infty} + \gamma_p V_{i\infty}^2) \quad (54)$$

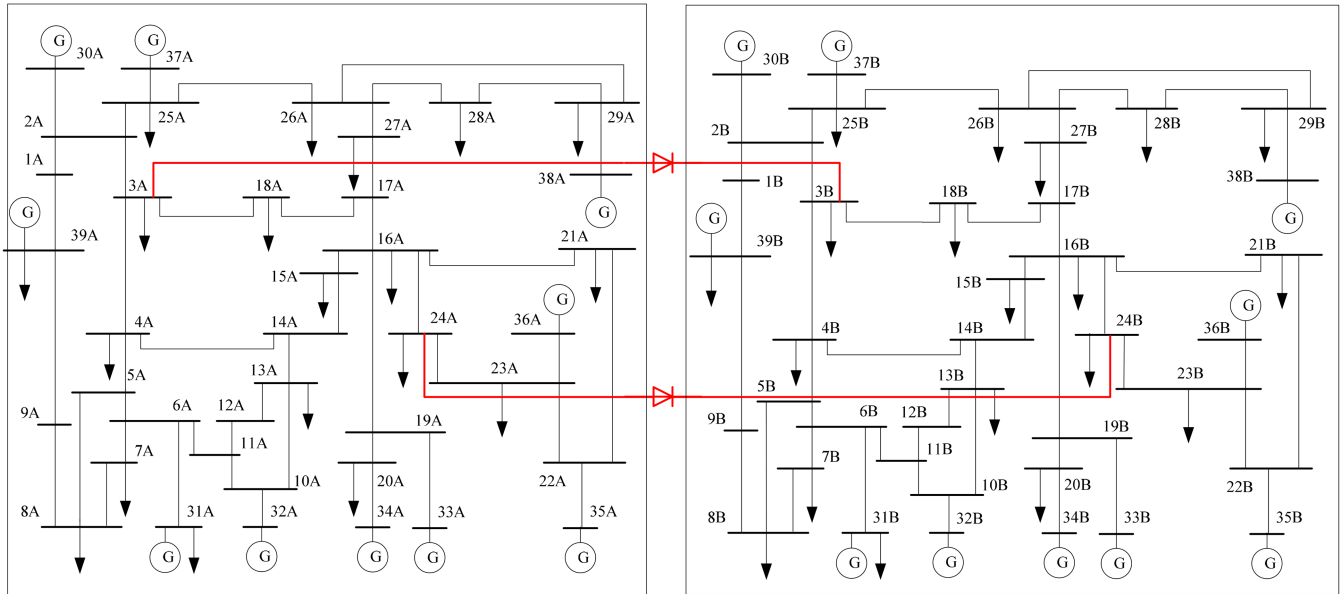


Fig. 7 Structure of the two-area AC/DC hybrid power system

$$B_{42} = \frac{\partial \Delta P_{Ri}}{\partial \Delta P_{du}^*} = \frac{V_{d0}^2}{\sqrt{(2R_d + V_{d0}^2)^2 + 4R_d V_{d0}^2 \Delta P_{du}^*}} \quad (55)$$

$$B_{51} = \frac{\partial \Delta Q_{Li}}{\partial \omega_1} = -q_0 K_{qt} (\alpha_q + \beta_q V_{i\infty} + \gamma_q V_{i\infty}^2) \quad (56)$$

11 Appendix C

See Fig. 7.